Investigation of Rotor Noise Source Mechanisms with Forward Speed Simulation

F.-R. Grosche* and H. Stiewitt†
Deutsche Forschungs-und Versuchsanstalt für Luft-und Raumfahrt E. V., Aerodynamische Versuchsanstalt Göttingen, Göttingen, W. Germany

The noise of a model propeller was measured with and without forward speed simulation in the open test section of a low-speed wind tunnel at velocities up to 60 m/s and blade tip Mach numbers up to 0.6. Compared to the static tests, even low wind velocities reduced the propeller noise by up to 20 dB. Strong sound radiation occurred due to interaction of the propeller blades with the wake of the supporting beam when the propeller was mounted as a pusher propeller. At wind velocities above 20 m/s, the high-frequency part of the propeller noise depends strongly on the angle of attack of the blades. At moderate angles of attack, laminar vortex shedding noise dominates the high-frequency sound radiation. This noise component could be eliminated by tripping the boundary layer on the suction surface of the blades. The frequencies of maximum noise radiation were predicted fairly well by existing theories. The laminar vortex shedding noise disappears at higher angles of attack of the propeller blades. If the angle of attack is further increased, strong braodband noise occurs which is generated probably by the turbulent boundary layer and local flow separations.

Nomenclature

c = blade chord (near the tip) = 0.029 m
d = propeller diameter = 0.414 m
f = frequency, Hz
f_0 = blade-passing frequency, Hz
h = camber of blade sections, m
L = sound pressure level, re 2×10^{-5} N/m^2, dB
M = Mach number
N = propeller speed, rps
r = radial position of blade sections, m
Re = Reynolds number, $Re = c\cdot U_{tip}/\nu$
t = maximum thickness of blade sections, m
U_∞ = wind velocity in the test section of the wind tunnel = forward speed, m/s
U_{tip} = helical blade tip velocity, $U_{tip} = [U_\infty^2 + (N\pi d)^2]^{1/2}$, m/s
x,y,z = Cartesian coordinates, m (see Fig. 2)
α = angle of attack of propeller blades (near the tip), deg
β = angular frequency of maximum instability of Tollmien-Schlichting waves, Hz
δ^* = boundary-layer displacement thickness, m
ϵ = pitch angle of propeller blades at the tip, deg
$\epsilon(r)$ = pitch angle at radial stations r, deg
ν = cinematic viscosity of air, m^2/s

I. Introduction

MEASUREMENTS of the sound radiation by propellers and helicopter rotors had been conducted earlier mainly through flight tests or, on the other hand, static tests without simulation of the forward speed of the aircraft. Quite often considerably higher noise levels were measured with static tests than with comparable flight tests (see, e.g., Refs. 1-4). This indicates that the sound-generating mechanisms can be affected significantly by the forward speed of the aircraft; therefore, static tests are only of limited value for the investigation of propeller and rotor noise under realistic flight conditions. On the other hand, flight tests are a rather expensive and time-consuming procedure, particularly if one intends to study the source mechanisms and possibilities of noise reduction. For this objective, model tests with forward speed simulation in a wind tunnel appear to be a suitable method. The present paper therefore describes some experiments to investigate the sound radiation of a model propeller in a wind-tunnel flow. In order to obtain a general survey of the effects of forward speed, measurements were made with a tractor-propeller and with a pusher-propeller configuration under static conditions and with main flow velocities up to 60 m/s.

Presented as Paper 77-1361 at the AIAA 4th Aeroacoustics Conference, Atlanta, Ga., Oct. 3-5, 1977; submitted Jan. 24, 1978; revision received Aug. 1, 1978.

Index category: Aeroacoustics.

*Scientist. Member AIAA.

†Scientist.

II. Apparatus

The noise radiation of a 4-bladed model propeller of a transport plane was measured in the open test section of the 3-m low-speed wind tunnel of the DFVLR-AVA Göttingen. The diameter of the propeller is 41.4 cm, characteristics of the propeller blades are listed in Table 1, and blade sections at different radial stations are plotted in Fig. 1. The pitch angle at the blade tip can be changed between 16 and 31.1 deg. A larger and a smaller propeller of the same type are also available for future scaling law tests. The propeller was driven by a high-speed electric motor in a streamlined nacelle mounted on a streamlined supporting beam.

A schematic view of the test setup is given in Fig. 2. The wind tunnel has a closed return circuit. The open test section is 6-m long and has a square nozzle with 3×3 m^2 exit area. The turbulence level in the test section is about 0.2%, the maximum wind velocity is 65 m/s. For a more detailed description of the tunnel see Refs. 5 and 6. The propeller nacelle was mounted on the axis of the test section 2.35 m downstream of the nozzle. An acoustic mirror microphone with a spherical mirror of 1-m diameter was used to scan the sound source distribution of the model and to discriminate the sound signal of the propeller from background noise. The measuring system and its calibration are described in detail in Ref. 7. The omnidirectional microphone shown in Fig. 2 was applied as a reference microphone in addition to the mirror system.

The tractor-propeller configuration indicated in Fig. 2 could be changed into a pusher-propeller configuration by turning the nacelle into the opposite direction and reversing the propeller on its axis. Figure 3 illustrates the test setup showing the propeller mounted as a tractor-propeller within the test section. The collector is on the left-hand side, the mirror microphone on its traversing unit and the om-

Table 1 Characteristics of the propeller blades, propeller diameter, $d = 414$ mm

Blade section, No.	Radial station, $r/(d/2)$	Blade chord, c, (cm)	Rel. blade thickness, t/c (%)	Camber ratio, h/c (%)	Pitch angle, $\epsilon(r)$, deg
1	1.0	2.88	2.2	1.7	31.1
2	0.95	2.96	3.1	2.1	32.6
3	0.84	3.10	4.6	2.7	35.8
4	0.74	3.25	6.1	3.1	39.3
5	0.64	3.05	8.2	3.2	43.4

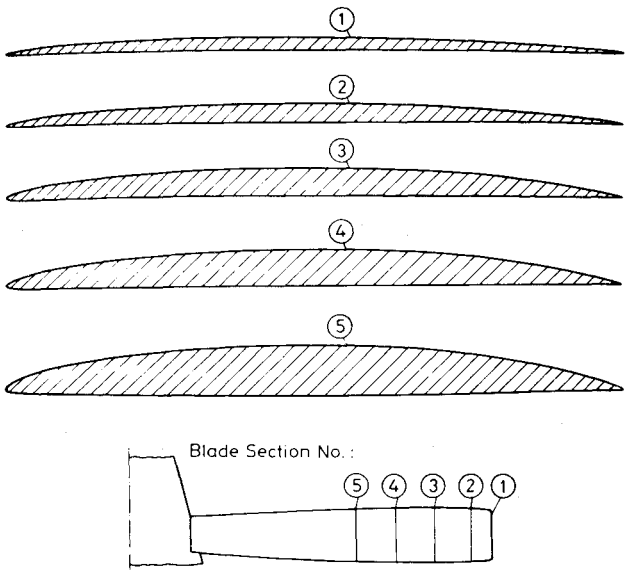

Fig. 1 Propeller blade sections at different radial positions.

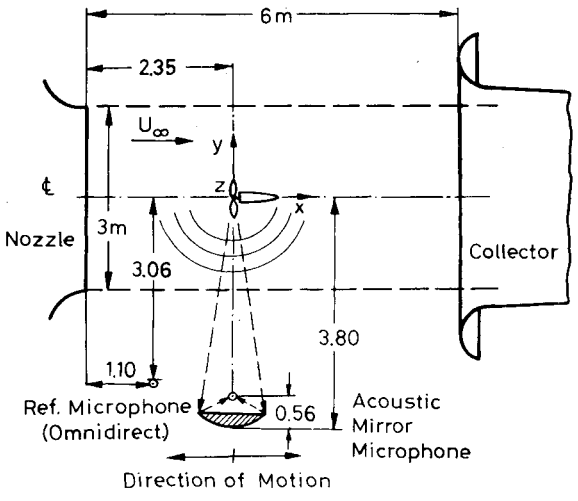

Fig. 2 Test setup.

nidirectional reference microphone are shown in the background. The ceiling, floor, and walls of the measuring chamber around the test section are treated acoustically to attain approximate free-field conditions for sound frequencies above 500 Hz.

Figure 4 presents a block diagram of the instrumentation. The propeller speed was measured and held constant during the runs. The signals of the mirror microphone and of the omnidirectional reference microphone—both were 1/4 in. B&K condenser microphones—could be analyzed by one-third octave filters or by a constant bandwidth real-time narrowband analyzer. Both methods were applied to most of the runs, but in this paper only the narrowband spectra will be discussed. In addition to the spectral analysis, the sound source distributions along the axis and normal to the axis of the nacelle could be determined in preselected one-third octave bands by traversing the mirror at constant speed and running the level recorder synchronously with the traversing unit. Details of the method are given in Ref. 7.

III. Measurements

Sound measurements with the acoustic mirror were made at approximately 90 deg to the propeller axis. The omnidirectional microphone was also located at a fixed position in the forward arc close to 70 deg from the propeller axis. Thus, no directivity patterns can be presented at this stage of the program.

The axial distribution of acoustic source intensity was investigated and narrowband and one-third octave frequency spectra of the propeller noise were measured at freestream velocities $0 \leqq U_\infty \leqq 60$ m/s and propeller speeds 30 rps $\leqq N \leqq 152$ rps. These speeds are equivalent to propeller tip Mach numbers between 0.1 and 0.6. The Reynolds numbers based on blade chord near the tip and tip velocity were in the range of $0.75 \times 10^5 < Re < 4 \times 10^5$.

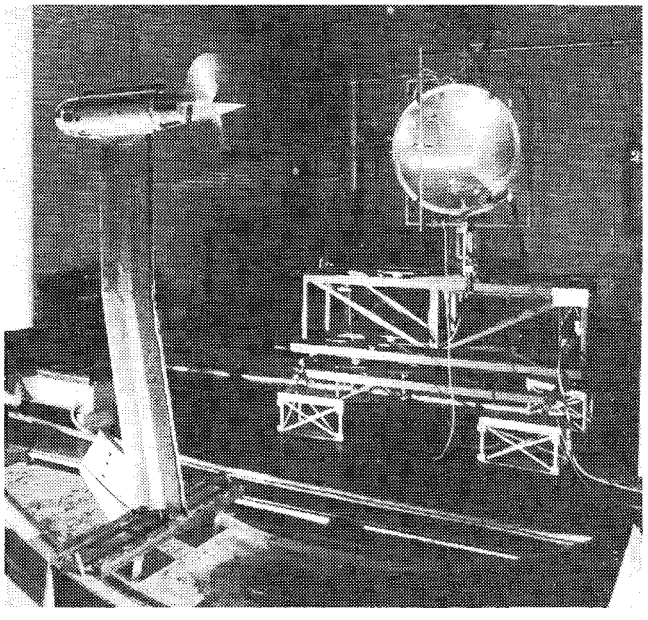

Fig. 3 Propeller and acoustic mirror microphone.

IV. Results

The following points will be discussed:

1) The distribution of the acoustic source intensity at the propeller nacelle combination.

2) The difference in sound radiation between tractor-propeller and pusher-propeller.

3) The difference in propeller noise between static tests and tests with low main flow velocity.

4) High-frequency propeller noise due to laminar vortex shedding and broadband noise caused by turbulent boundary-layer and flow separation.

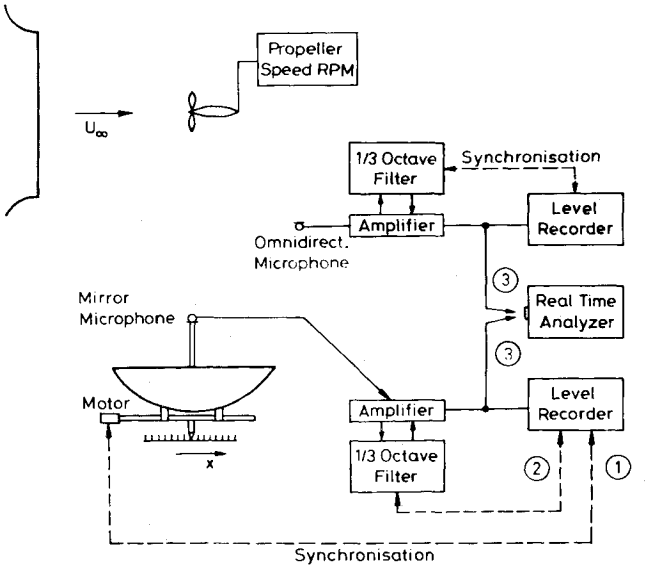

Fig. 4 Block diagram of the instrumentation.

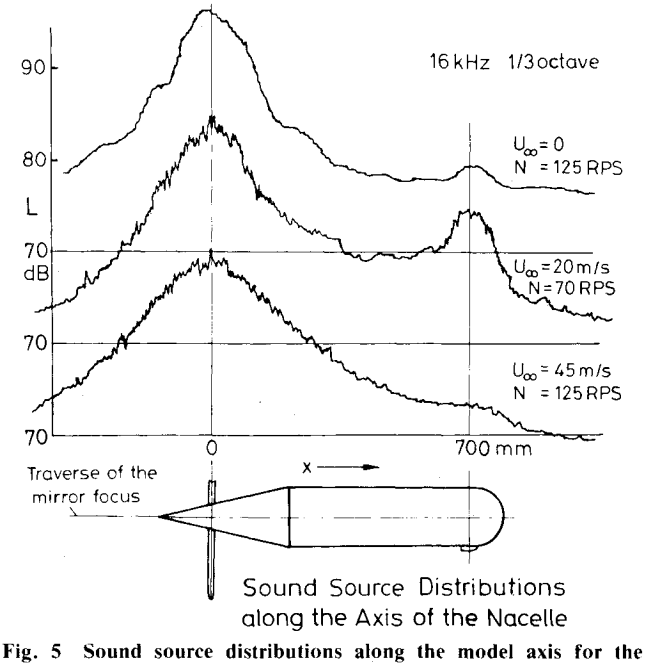

Fig. 5 Sound source distributions along the model axis for the tractor-propeller configuration.

A. Axial Source Distribution at the Propeller Nacelle

Figure 5 gives some typical distributions of sound-source intensity along the axis of the propeller nacelle measured in the 16 kHz one-third octave band at different main flow velocities U_∞ and propeller speeds N. The measured data have been corrected only for the apparent downstream shift of the source locations, due to the convection and refraction of sound waves by the wind-tunnel flow according to Ref. 7. The variations of gain and spatial resolution of the mirror with wind velocity (see Ref. 7) were not considered yet in this graph, which therefore only indicates the positions and relative strength of the sound sources for the different flow conditions. The main question was if the electric motor within the nacelle or the flow noise at the surface of the nacelle would contribute significantly to the total noise output. Figure 5 demonstrates that the noise of the propeller dominates the source distribution. A much weaker secondary peak of sound radiation was sometimes observed at the nacelle about 70 cm from the propeller, see e.g. the second curve of Fig. 5. There are some openings for electric wires and

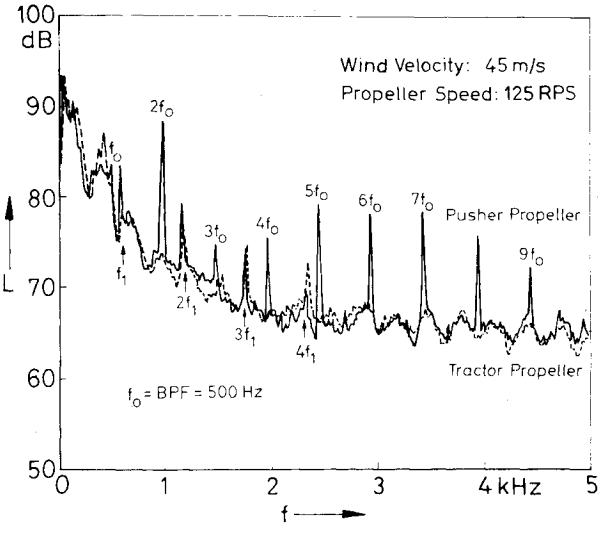

Fig. 6 Difference in sound radiation between tractor-propeller and pusher-propeller; blade pitch $\epsilon = 16.1$ deg, analyzer bandwidth: 10 Hz.

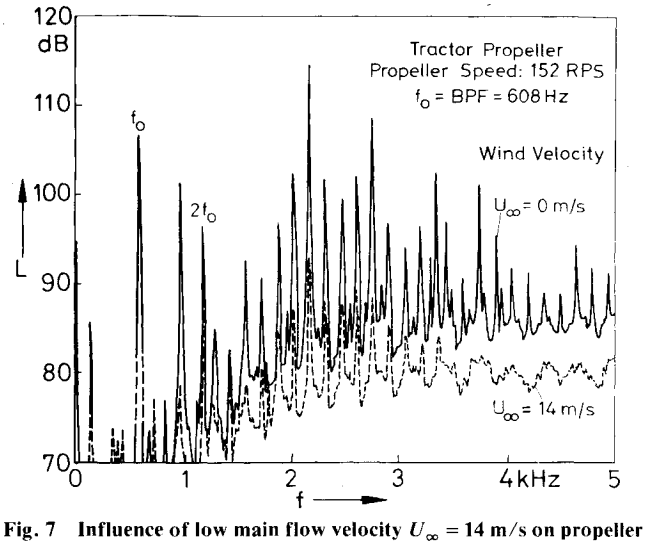

Fig. 7 Influence of low main flow velocity $U_\infty = 14$ m/s on propeller noise; blade pitch $\epsilon = 16.1$ deg, analyzer bandwidth: 10 Hz.

cooling water hoses in the nacelle surface at this location and it is believed that the noise coming from there may be either noise of the electric motor or, more probably, flow noise caused by the holes and protuberances at this position. The results for the pusher-propeller configuration are quite similar to the curves for the tractor-propeller given in Fig. 5.

B. Comparison Between Tractor-Propeller and Pusher-Propeller Noise

While the tractor-propeller has a fairly smooth and steady inflow, the pusher-propeller operates in the wakes of both the motor-nacelle and the supporting beam shown in Fig. 3. Particularly the wake of the supporting beam, since extending over the entire length of the propeller blades is bound to induce a strong impulsive blade loading which, according to Ref. 8 and other authors, should generate intense discrete frequency sound at a number of harmonics of the blade-passing frequency. This was well confirmed by our test results. As an example, Fig. 6 presents narrowband spectra of the tractor-propeller and the pusher-propeller configurations at wind velocity $U_\infty = 45$ m/s and propeller speed $N = 125$ rps. The blade-passing frequency is f_0; the frequency f_1 and its harmonics are not related to the propeller noise but to the noise of the wind-tunnel drive. The harmonics of f_0 are up to 15 dB higher for the pusher-propeller than for the tractor-propeller. The magnitude of this effect appears to be

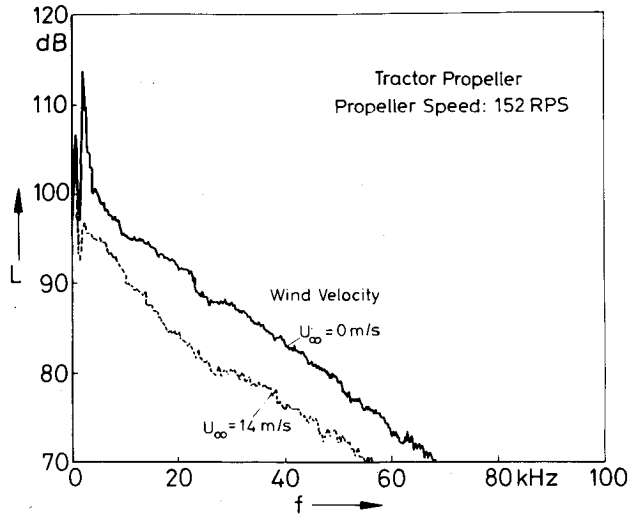

Fig. 8 Influence of low main flow velocity $U_\infty = 14$ m/s on propeller noise; blade pitch $\epsilon = 16.1$ deg, analyzer bandwidth: 200 Hz.

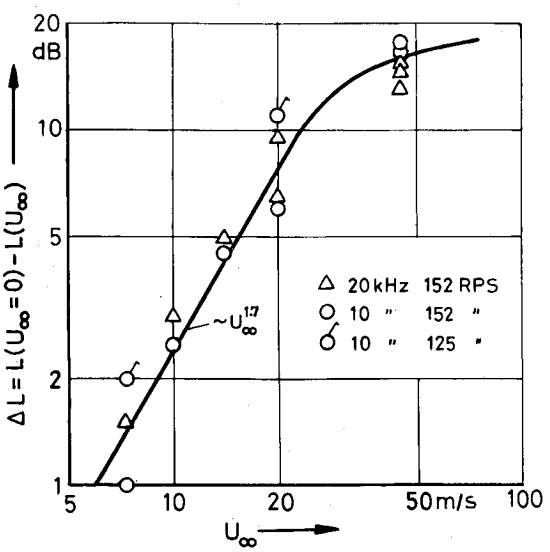

Fig. 9 Reduction of propeller noise with increasing main flow velocity.

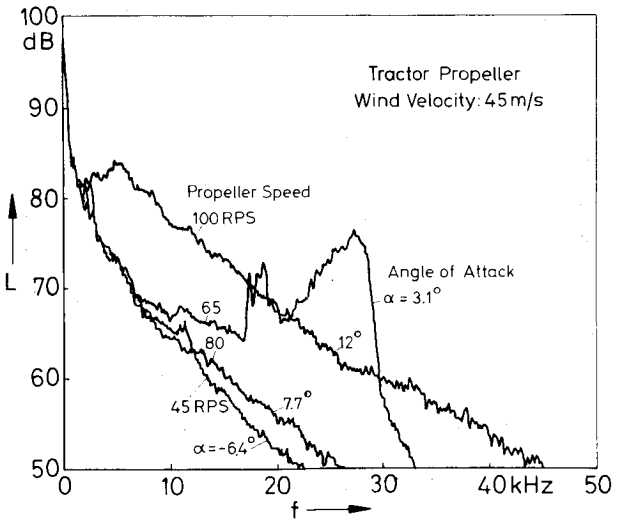

Fig. 10 Influence of propeller speed and angle of attack on noise at constant main flow velocity $U_\infty = 45$ m/s; blade pitch $\epsilon = 31.1$ deg, analyzer bandwidth: 100 Hz.

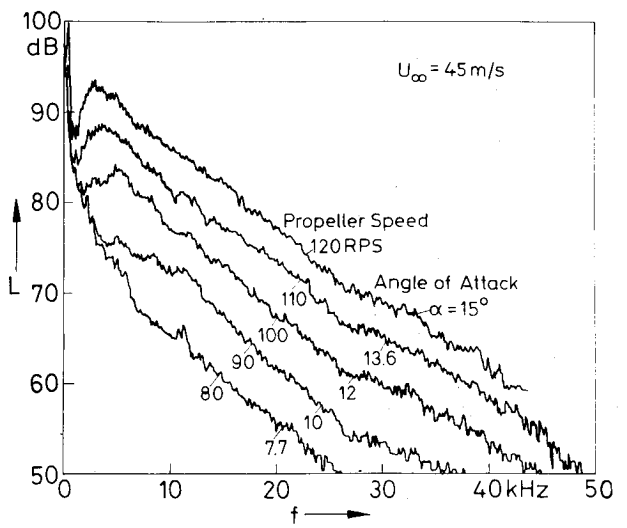

Fig. 11 Influence of high angles of attack on propeller noise at constant main flow velocity $U_\infty = 45$ m/s; tractor-propeller, blade pitch $\epsilon = 31.1$ deg, analyzer bandwidth: 100 Hz.

remarkable considering that the nacelle and the supporting beam are fairly well streamlined and that the distance of the supporting beam from the propeller was more than 30 cm or 10 chord lengths of the blades. A survey of the wake and comparison of the test results with predictions[8] will be carried out in the near future.

C. Effect of Low Main Flow Velocities on Propeller Noise

Measurements at low wind velocities $0 \leqq U_\infty \leqq 20$ m/s were conducted to obtain new evidence concerning the observed differences in propeller noise between static and flight tests (see Refs. 1-4 and 8-10). As an example, constant bandwidth narrowband spectra measured with the mirror microphone system at zero wind velocity and at $U_\infty = 14$ m/s are plotted together in Fig. 7. The levels are approximately equal at the blade-passing frequency f_0, but differ strongly at the higher harmonics. With main flow, the sound pressure levels are 10-20 dB lower than without wind. The marked reduction of the propeller noise with increasing flow velocity is clearly audible, by the way, if one stands in the vicinity of the model while the wind tunnel is started. Figure 8 demonstrates that a similar, although somewhat smaller, difference between the static test and tests with low main flow velocity exists also at higher sound frequencies.

The dependence of the noise reduction on main flow velocity U_∞ is given in Fig. 9 for the arbitrarily selected frequencies $f = 10$ and $f = 20$ kHz, with ΔL being the noise reduction compared to the static tests. The graph shows ΔL to increase approximately with main flow velocity to the 1.7 power until it levels off at wind velocities $U_\infty > 20$ m/s. This reduction in propeller noise is probably caused by the following effects:

1) Vortex stretching of inflowing turbulence is diminished as wind velocity increases (compare Refs. 2, 4, and 10).

2) Recirculation of propeller turbulence back into the propeller plane is reduced (see Refs. 8 and 11).

3) The angle of attack at the propeller blades is reduced and thus the possibility of local flow separations is decreased.

Further evaluation of the data and probably additional measurements are required to obtain a clearer picture of the mechanisms involved.

D. Laminar Vortex Shedding Noise and Broadband Noise at High Angles of Attack

Narrow-band spectra of the propeller noise measured by the mirror microphone at constant wind velocity $U_\infty = 45$ m/s and various propeller speeds between $N = 45$ rps and $N = 100$ rps are presented in Fig. 10. Similar measurements were made at other wind velocities and propeller speeds.

Obviously, the high-frequency part of the noise depends strongly on propeller speed which, at constant wind velocity,

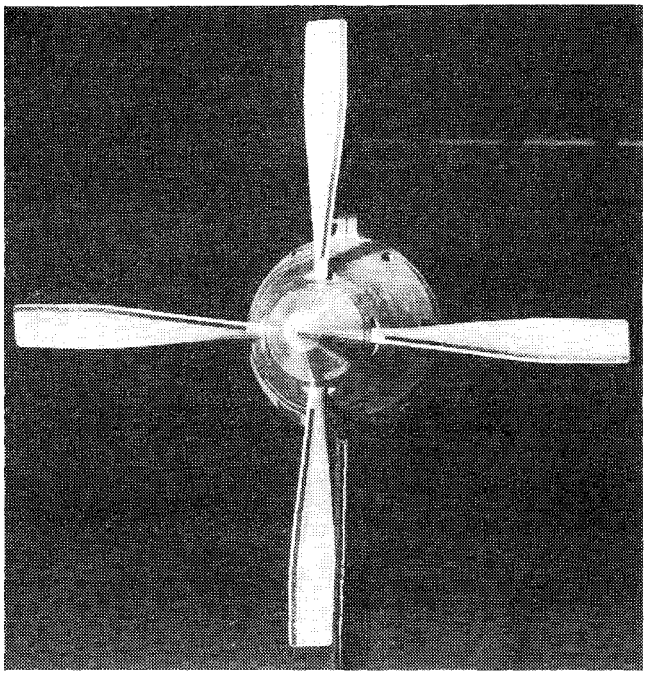

Fig. 12 Propeller with strips of adhesive tape on the suction surface near the leading edge of the blades to trip the laminar boundary layer.

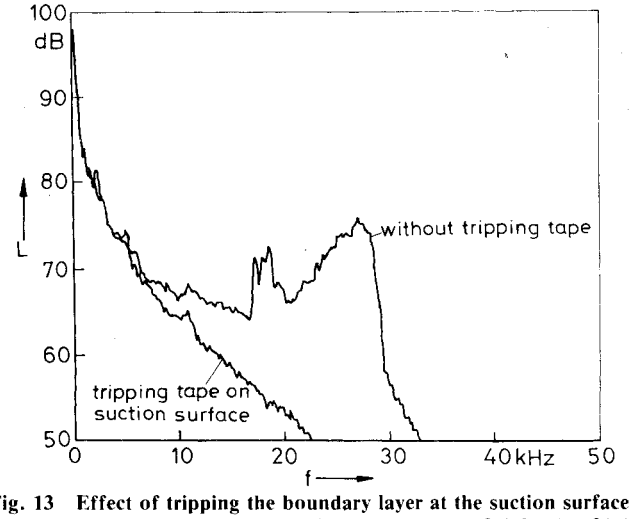

Fig. 13 Effect of tripping the boundary layer at the suction surface of the propeller blades, $U_\infty = 45$ m/s, $N = 65$ rps, $\alpha = 3.1$ deg ($\epsilon = 31.1$ deg); analyzer bandwidth: 100 Hz.

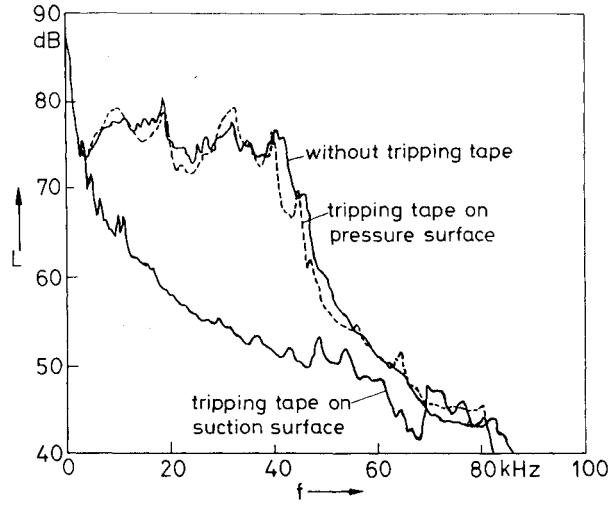

Fig. 14 Effect of tripping the boundary layer at the suction surface or at the pressure surface, $U_\infty = 30$ m/s, $N = 90$ rps, $\alpha = 1.7$ deg ($\epsilon = 16.1$ deg), analyzer bandwidth: 200 Hz.

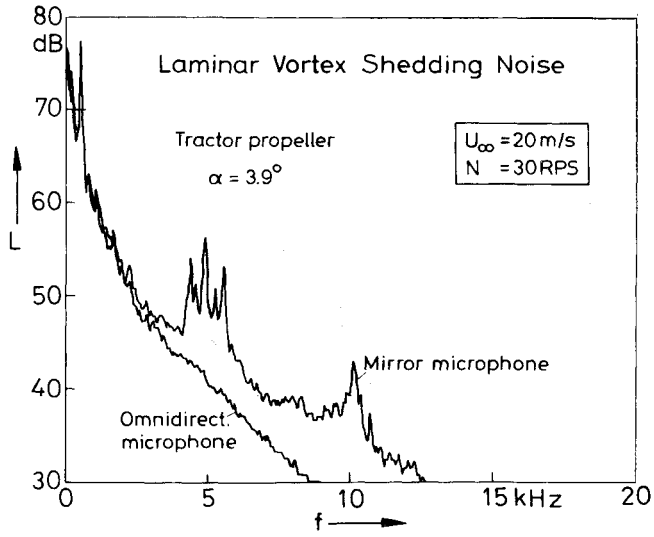

Fig. 15 Narrowband spectra measured at $U_{tip} = 44$ m/s, $Re = 9 \times 10^4$, $\alpha = 3.9$ deg ($\epsilon = 31.1$ deg), analyzer bandwidth: 40 Hz.

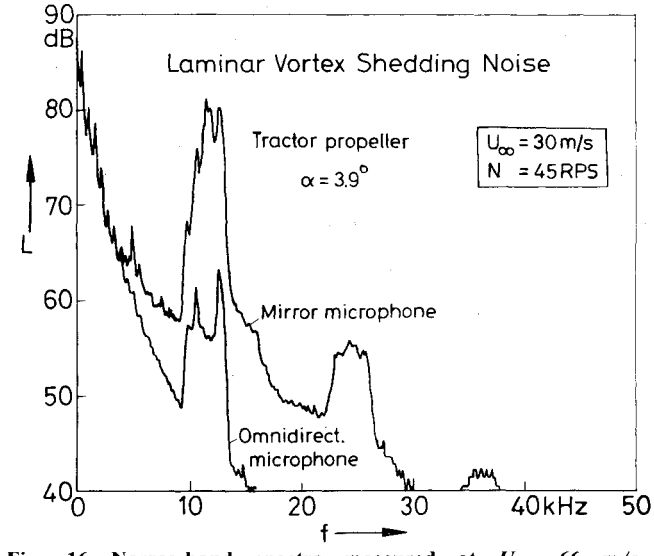

Fig. 16 Narrowband spectra measured at $U_{tip} = 66$ m/s, $Re = 1.3 \times 10^5$, $\alpha = 3.9$ deg ($\epsilon = 31.1$ deg), analyzer bandwidth: 100 Hz.

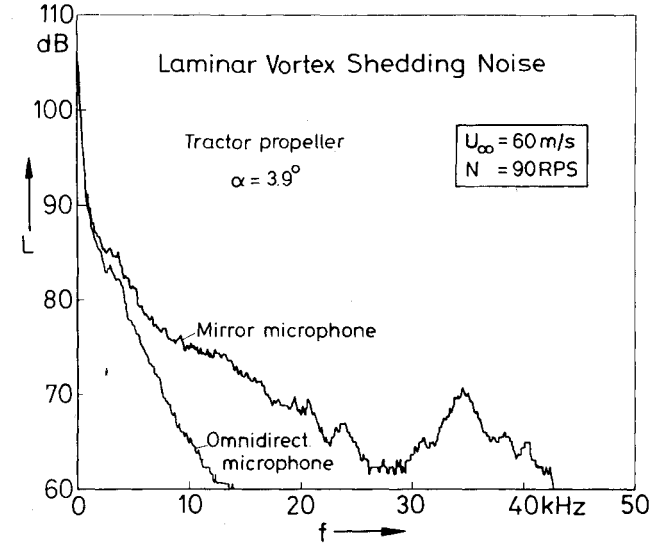

Fig. 17 Narrowband spectra measured at $U_{tip} = 132$ m/s, $Re = 2.6 \times 10^5$, $\alpha = 3.9$ deg ($\epsilon = 31.1$ deg), analyzer bandwidth: 100 Hz.

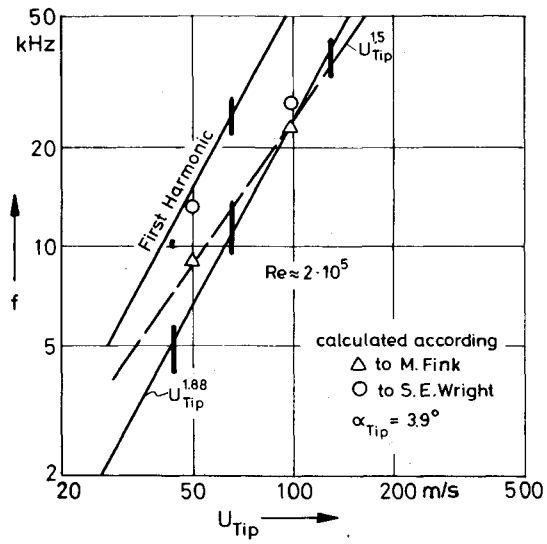

Fig. 18 Peak frequencies of lamainar vortex shedding noise as function of effective blade tip velocity U_{tip} for constant angle of attack $\alpha = 3.9$ deg.

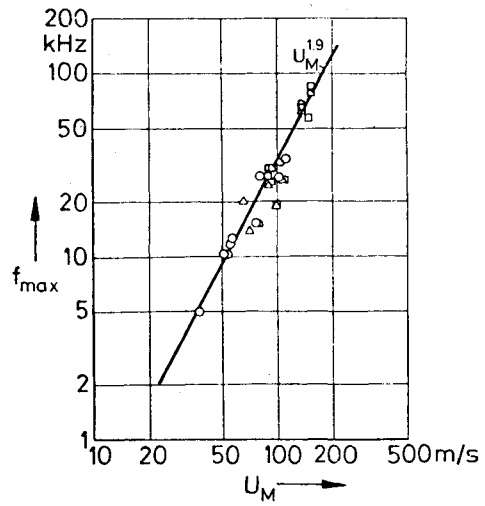

Fig. 19 Peak frequencies of laminar vortex shedding noise as function of effective blade speed U_M.

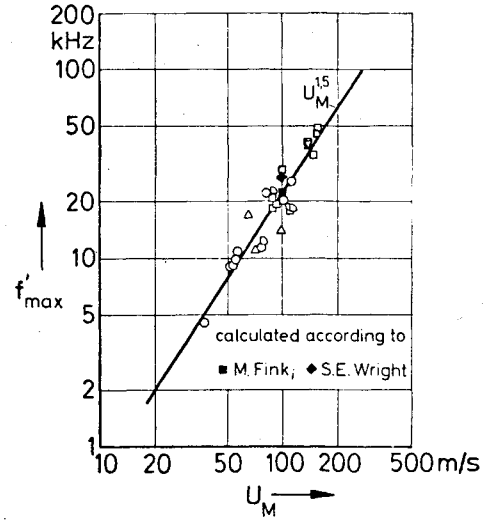

Fig. 20 Peak frequencies of laminar vortex shedding noise corrected for Doppler shift.

also determines the angle of attack near the tip of the blades. At $N = 45$ rps, $\alpha = -6.4$ deg and at $N = 80$ rps, $\alpha = 7.7$ deg, the spectrum shape is quite similar, the level decreasing rapidly with increasing frequency. In between these propeller speeds or angles of attack is a region where strong peaks occur in the spectrum. As an example, the spectrum measured at $N = 65$ rps, $\alpha = 3.1$ deg is plotted in Fig. 10. It shows two maxima at approximately 18 and 28 kHz. The level of the second peak is about 25 dB higher than the level of the spectrum measured at $N = 80$ rps, $\alpha = 7.7$ deg.

If the propeller speed and thus the angle of attack is further increased, the level of the entire spectrum above 2 kHz raises continuously. This is illustrated by Fig. 11 and by the corresponding spectrum for $N = 100$ rps, $\alpha = 12$ deg in Fig. 9. The peak frequencies of the broadband noise spectra agree reasonably well with the prediction given by Wright for turbulent boundary-layer noise (see Eq. 5.2 in Ref. 8).

$$f_t = S_t \cdot U_{tip}/c \tag{1}$$

where the Strouhal number S_t is approximately unity, but decreases slightly with increasing angle of attack. This fact and the rapid rise of the spectra with increasing α suggest that the intense broadband noise observed for angles of attack, $\alpha \geqq 10$ deg, is due to the turbulent boundary layer and to turbulent flow separation from the propeller blades.

The strong peaks occurring in the spectrum at moderate angles of attack (see the curve for $\alpha = 3.1$ deg in Fig. 10) were related to oscillations of the laminar boundary layer at the blades. To check this assumption, narrow strips of adhesive tape were positioned on the suction surface of the blades close to the leading edge as illustrated by Fig. 12, in order to trip the laminar boundary layer. The effect of this measure is demonstrated by Fig. 13. The high-frequency peaks are suppressed completely by the tripping of the boundary layer. The Reynolds number based on blade chord and effective velocity at the tip was approximately 2×10^5. The result strongly suggests that the observed peaks are laminar boundary layer or laminar vortex shedding noise which has been studied earlier—mainly with stationary isolated airfoils immersed in a wind-tunnel flow—by Patterson et al.[12] and other investigators, e.g., Refs. 8 and 13-15. Only in their experiments was the laminar boundary layer at the pressure surface found to be responsible for the peaks in the sound spectrum. We therefore performed some other tests fixing the tripping tape alternatively at the suction or at the pressure surface of the blades. One example is presented in Fig. 14; the Reynolds number was $Re = 2.3 \times 10^5$ in this case. The tape fixed to the pressure surface did not significantly influence the sound spectrum. Only the tape fixed to the suction surface was effective. The same result was found at other flow conditions with similar or lower Reynolds numbers. Laminar vortex shedding noise from the suction surface of cambered fan blades at small negative angles of incidence has also been observed recently by Longhouse.[16] In his experiments, the boundary layer at the pressure surface was turbulent because of the adverse pressure gradient downstream of a suction peak close to the leading edge.

It remains open if in our case the ineffectiveness of boundary-layer trips at the pressure surface was due to the same effect.

The dependence of the laminar vortex shedding noise on effective blade tip velocity U_{tip} for constant angle of attack α is illustrated by Figs. 15-17 showing narrowband spectra obtained with the mirror microphone and with the omnidirectional reference microphone for $\alpha = 3.9$ deg and different velocities U_{tip}. At the lowest velocity $U_{tip} = 44$ m/s corresponding to a Reynolds number $Re \approx 0.9 \times 10^5$, a region of laminar vortex shedding noise can be identified around 5 kHz in the mirror microphone spectrum of Fig. 15 with a first harmonic at approximately 10 kHz. The spectrum of the omnidirectional microphone is dominated by the background noise of the tunnel which masks the sound signal of the propeller. Figure 16 gives the spectra at a 50% higher velocity $U_{tip} = 66$ m/s, $Re \approx 1.3 \times 10^5$. The laminar vortex shedding

noise is particularly pronounced at this flow condition, exceeding the broadband components by more than 20 dB. Therefore, it can also be observed in the spectrum of the omnidirectional microphone. The frequencies of the major peak and its first harmonic are shifted to approximately 12 and 25 kHz. A second harmonic is just detectable at about 37 kHz. The spectra measured with $U_{tip} = 132$ m/s, $Re \approx 2.6 \times 10^5$ are plotted in Fig. 17. The laminar vortex shedding noise is lower than in the previous diagram, the peak frequency is close to 35 kHz.

The acoustic wave length λ of the laminar vortex shedding sound is almost exactly equal to the blade chord c in the case of Fig. 16, where this noise component is particularly strong. For Figs. 15 and 17, the ratio c/λ is 0.42 and 2.9, respectively. The observed intensity variation of the laminar vortex noise with c/λ seems to support the acoustic feedback model of Ref. 8. Similar results are reported in Refs. 12 and 13 for isolated airfoils in a uniform flow.

The frequency bands of the laminar vortex noise peaks of Figs. 15-17 are presented in Fig. 18 as a function of the effective tip speed U_{tip} of the propeller blades. The peak frequencies vary approximately $\sim U_{tip}^{1.9}$. For comparison, laminar boundary-layer tone frequencies were calculated by means of the theory of Fink.[17] Using Eq. (2) of Ref. 17.

$$f = \frac{1}{2\pi \cdot 1.73} \cdot \frac{\beta\delta^*}{U_{tip}} \cdot \frac{U_{tip}^{3/2}}{(c\nu)^{1/2}} \tag{2}$$

with the reduced frequency $(\beta\delta^*/U_{tip}) \approx 0.17$ according to Fig. 1 of Ref. 17, the theoretical curve (dashed line) plotted in Fig. 18 was obtained. Two values of another rather crude estimate based on Eq. (4.13) of Ref. 8 by Wright

$$f = S \cdot U_{tip}/c \tag{3}$$

with Strouhal number $S \approx 8$ are also given in Fig. 18. A greater number of peak frequencies measured at different angles of attack are plotted in Fig. 19 over U_M, which is the relative velocity at 0.8 of the tip radius of the blades. Again a $U^{1.9}$ power law is indicated by the test results. The reason for this discrepancy to the theoretical power law $U^{1.5}$ was found to be the Doppler shift of the radiated sound frequencies, due to the motion of the blades toward the mirror microphone. If the observed peak frequencies are corrected for this Doppler shift by

$$f' = f\left(1 - \frac{U_M}{a_0}\right) \tag{4}$$

the measurements agree very well with the theoretical predictions by Fink[17] and Wright.[8] This is demonstrated by Fig. 20.

V. Conclusions

Tests with a model propeller in a wind-tunnel flow were conducted to investigate forward speed effects on the sound-generating mechanisms.

1) A survey of the distribution of sound source intensities at the propeller nacelle established that the propeller itself was the dominating source of noise.

2) Considerable amplification of the harmonics of the blade-passing frequency was observed due to interaction of the propeller with the wake of nacelle and supporting beam if the model was operated as a pusher-propeller.

3) Low main flow velocities $U_\infty \leqq 20$ m/s reduced the rotational noise and the high-frequency broadband noise of the propeller by up to 20 dB as compared to static tests.

4) The high-frequency part of the propeller noise spectrum was found to depend markedly on the angle of attack of the blades for main flow velocities $U_\infty \geqq 20$ m/s. Laminar vortex shedding noise dominated the sound radiation for moderate angles of attack. This noise component could be suppressed by tripping the laminar boundary layer on the suction surface of the blades. The peak frequencies agreed fairly well with theoretical estimates. The laminar vortex shedding sound disappeared at higher angles of attack, $\alpha \approx 8$ deg. Strong broadband noise probably was generated by the turbulent boundary-layer and flow separations if the angle of attack of the propeller blade was further increased. The peak frequency of the broadband noise was also in satisfactory agreement with predictions.

The results obtained thus far essentially validate and extend the knowledge gained by earlier investigations of rotor noise. Further evaluation of the data and additional measurements are required for a better understanding of the noise-generating mechanisms.

References

[1] Regier, A. A. and Hubbard, H. H., "Factors Affecting the Design of Quiet Propellers," NACA RM No. L7H05, 1947.

[2] Hanson, D. B., "A Study of Subsonic Fan Noise Sources," AIAA Paper 75-468, 1975.

[3] van Deventer, F. W. J. and Ruijgrok, G.J.J., "External Noise of Light Propeller-Driven Aircraft," ICAS Paper 76-48, 1976.

[4] Metzger, F. B., Magliozzi, B., and Pegg, R. J., "Progress Report on Propeller Aircraft Flyover Noise Research," SAE Paper 760454, 1976.

[5] Riegels, F. W. and Wuest, W., "Der 3-m-Windkanal der Aerodynamischen Versuchsanstalt Göttingen," Z. Flugwiss, 9, 1961, pp. 222-228.

[6] Fütterer, H., Mehmel, D., and Riegels, F. W., "Messtechnik, Datenerfassung und Datenverarbeitung an den grossen Windkanälen der Aerodynamischen Versuchsanstalt Göttingen," Jb. DGLR 1970, 1971, pp. 166-185.

[7] Grosche, F.-R., Stiewitt, H., and Binder, B., "On Aero-Acoustic Measurements in Wind Tunnels by Means of a Highly Directional Microphone System," AIAA Paper 76-535, 1976; also *AIAA Journal*, Vol. 15, Nov. 1977, pp. 1590-1596.

[8] Wright, S. E., "The Acoustic Spectrum of Axial Flow Machines," *Journal of Sound and Vibration*, Vol. 45, Feb. 1976, pp. 165-223.

[9] Bartels, P., "Untersuchungen zur Lärmreduzierung von Propellerflugzeug-Antrieben," Dornier Bericht 75/8/B, 1975.

[10] Metzger, F.B. and Magliozzi, B., "New Directions in Aircraft Propulsor Noise Research," SAE Paper 750515, 1975.

[11] Lowson, M.V., Whatmore, A., and Whitfield, C. E., "Source Mechanisms for Rotor Noise Radiation," Univ. of Tech. Loughborough, TT 7207, 1972.

[12] Paterson, R. W., et al., "Vortex Noise of Isolated Airfoils," *Journal of Aircraft*, Vol. 10, May 1973, pp. 296-302.

[13] Schlinker, R. H., Fink, M. R., and Amiet, R. K., "Vortex Noise from Nonrotating Cylinders and Airfoils," AIAA Paper 76-81, 1976.

[14] Soderman, P. T., "Leading-Edge Serrations which Reduce the Noise of Low-Speed Rotors," NASA TN D-7371, 1973.

[15] Lyon, C. A., Shahady, P. A., and Elrod, W. C., "Propeller Acoustics Research (Isolated Airfoil Noise)," AFA PL-TR-78, 1975.

[16] Longhouse, R. E., "Vortex Shedding Noise of Low Tip Speed, Axial Flow Fans," *Journal of Sound and Vibration*, Vol. 53, Jan. 1977, pp. 25-46.

[17] Fink, M. R., "Prediction of Airfoil Tone Frequencies," *Journal of Aircraft*, Vol. 12, Feb. 1975, pp. 118-119.